Chem

CellPress
OPEN ACCESS

Article

Enhanced coherence by coupling spins through a delocalized π-system: Vanadyl porphyrin dimers

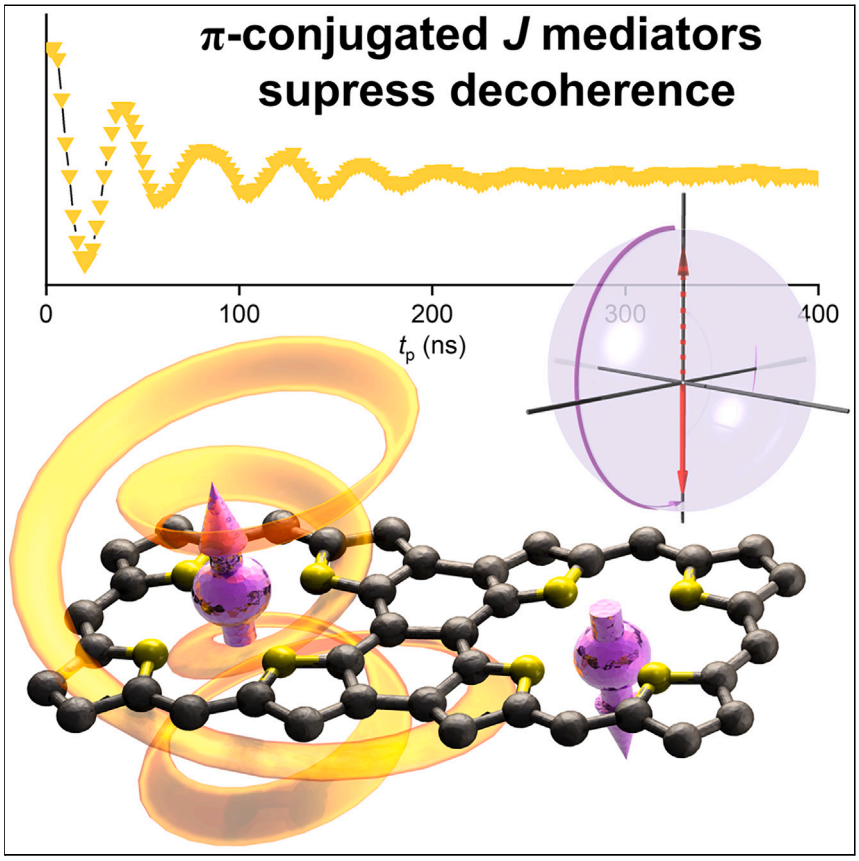

In the field of molecular quantum technologies, it is desirable to connect spin centers with both electronic and magnetic communication channels. We address this problem by embedding paramagnetic vanadyl centers in porphyrin arrays. A strongly π-conjugated backbone places the magnetic system in an intermediate regime dominated by exchange coupling, suppressing decoherence at temperatures below 4 K. This behavior should be valuable for the design of molecular devices controlled by microwaves with electrical readout.

Iago Pozo, Zhijie Huang, Federico Lombardi, ..., William K. Myers, Lapo Bogani, Harry L. Anderson

iago.pozomiguez@chem.ox.ac.uk (I.P.)
lapo.bogani@materials.ox.ac.uk (L.B.)
harry.anderson@chem.ox.ac.uk (H.L.A.)

Highlights

A range of π-conjugated bis-vanadyl porphyrin dimers have been synthesized

Strong π-conjugation places vanadyl porphyrin dimers in the *J*-dominated regime

Dominant exchange coupling suppresses decoherence from electron flip-flop processes

Magnetic porphyrin polymers are promising for quantum information processing

Pozo et al., Chem *10*, 1–18
January 11, 2024
Published by Elsevier Inc.
https://doi.org/10.1016/j.chempr.2023.09.013

Please cite this article in press as: Pozo et al., Enhanced coherence by coupling spins through a delocalized π-system: Vanadyl porphyrin dimers, Chem (2023), https://doi.org/10.1016/j.chempr.2023.09.013

Chem

CellPress
OPEN ACCESS

Article

Enhanced coherence by coupling spins through a delocalized π-system: Vanadyl porphyrin dimers

Iago Pozo,[1,2,*] Zhijie Huang,[1,7] Federico Lombardi,[1,7] Dimitris I. Alexandropoulos,[1] Fanmiao Kong,[1] Michael Slota,[1] Igor Tkach,[3] Marina Bennati,[3,4] Jie-Ren Deng,[2] Wojciech Stawski,[2] Peter N. Horton,[5] Simon J. Coles,[5] William K. Myers,[6] Lapo Bogani,[1,*] and Harry L. Anderson[2,8,*]

SUMMARY

Vanadium(IV) magnetic centers are prime candidates for molecular quantum units. One long-standing question is how to obtain a scaffold that connects multiple centers and allows two communication modalities: magnetic and electronic. We have synthesized and studied a selection of vanadyl porphyrin dimers as models of the most synthetically accessible linear porphyrin arrays. We show that a strongly π-conjugated backbone places the magnetic system in an intermediate regime dominated by exchange coupling (*J*) and protects the quantum coherence against electron pair flip-flop processes at low temperatures (<10 K). This result is a fundamental step toward the design of molecular materials for single-molecule devices controlled by microwaves with electrical readout.

INTRODUCTION

Transition metal complexes offer many examples of interesting magnetic behavior. For example, V^{4+} complexes[1–4] (particularly vanadyl derivatives)[5–8] have long coherence times,[9,10] hyperfine coupling in a range suitable for microwave manipulation,[11] and the possibility of creating air-stable complexes and tunable scaffolds.[10] A central question is how to achieve magnetic coupling between multiple metal centers via a molecular backbone. The development of scaffolds that allow the transfer of electrons and that can be extended to multiple centers by direct chemical design is urgently needed. Although electron transport is facilitated by the presence of delocalized π-orbitals in organic materials, the influence of a conjugated backbone on the magnetic properties remains difficult to anticipate. The proximity of several spin centers often has detrimental effects on the quantum coherence.[12–15] Whether the addition of multiple centers to a quantum system will inevitably lead to a transition from quantum to classical behavior, and at what scale, is still a matter of speculation. In this context, it is interesting that some non-molecular systems, e.g., Si quantum dots and Ti atoms, do not display increased decoherence when exchange coupling of spins occurs via specific quantum mediators.[16–21] Although a single spin is easily disrupted by magnetic noise, a coupled-spin system can resist decoherence, if the right conditions are met. Theoretical work shows that Bell states of coupled two-level spin systems exhibit coherence lifetime enhancement correlated to exchange interaction amplitudes under a range of Markovian and non-Markovian noise conditions. In essence, noise induces state-switching oscillations, and exchange interactions alter the spin

THE BIGGER PICTURE

Units of quantum information, called qubits, must communicate with each other if they are to perform useful logic operations. Finding suitable scaffolds for linking chemically synthesized qubits together is crucial for the development of molecular quantum technologies. π-conjugated linkers allow efficient electron transport over relatively long distances, but can they be used to couple together qubits, such as vanadyl ions?

In this article, we not only answer affirmatively but also show that conjugated linkers can outperform other types of bridges by preserving the quantum coherence. We synthesize two families of porphyrins containing vanadyl ions and investigate their geometry, conjugation, and quantum performance. The discovery that a π-conjugated backbone can protect from decoherence is valuable for the design of molecular materials for functional quantum devices operated by microwaves and with electrical readout.

Please cite this article in press as: Pozo et al., Enhanced coherence by coupling spins through a delocalized π-system: Vanadyl porphyrin dimers, Chem (2023), https://doi.org/10.1016/j.chempr.2023.09.013

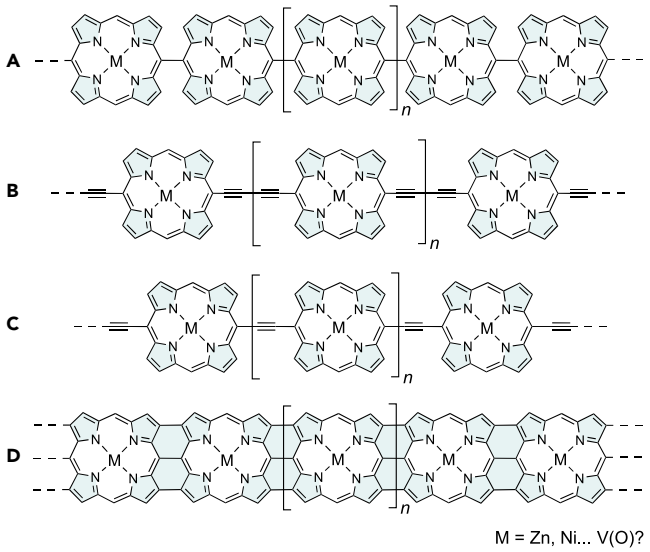

Figure 1. Examples of polymeric porphyrin backbones, in order of increasing π-delocalization

Porphyrin polymers that are (A) singly linked, (B) butadiyne linked, (C) ethyne linked, and (D) edge fused.

Solubilizing side chains not shown.

precession to keep the trajectory close to the initial state, even in the presence of noise.[18] It is difficult to predict which systems meet the prerequisites for coherence protection, but experimental observations on quantum dots indicate that the effect can arise in two-dimensional (2D) electron gases.[20,21] In molecular systems, π-conjugated bridges could produce a similar effect, and this would open major avenues for the rational design of molecular quantum materials.[22,23] With the purpose of exploring this issue, molecular magnets have been immobilized onto or into carbon nanotubes,[24–30] and π-conjugated backbones have been combined with magnetic centers, such as open-shell graphenoids[31–33] or graphene nanoribbons.[34,35] In this context, π-conjugated porphyrin polymers[36–44] appear to be ideal scaffolds. They offer a single delocalized channel linking multiple metallic centers, such as copper(II)[45–47] or lanthanides,[48,49] each placed at a precise distance and location.

Zinc(II) porphyrin oligomers have been widely investigated as molecular wires.[36–44] The chemical structures of the most synthetically accessible porphyrin polymers, all of which could potentially be synthesized with vanadyl centers, are shown in Figure 1. Two experimental approaches have been used to probe the strength of π-conjugation in these oligomers: (1) measurement of the UV-vis-NIR spectra of discrete oligomers, to test how the HOMO-LUMO gap (i.e. the energy difference between the highest occupied molecular orbital and the lowest unoccupied molecular orbital) decreases with increasing chain length[38,39] and (2) measurement of the single-molecule conductances, to evaluate the attenuation of conductance as a function of molecular length.[42–44] Both approaches show that the polymers represented in Figure 1 exhibit increasingly strong π-delocalization in the order A < B < C < D. Singly *meso-meso*-linked chains (A) are not π-conjugated because the planes of neighboring porphyrins are almost orthogonal, whereas edge-fused chains (D) have highly delocalized electronic structures. To date, the influence of π-conjugation on the quantum coherence of vanadyl units in porphyrin arrays remains elusive, despite recent studies of edge-fused and singly linked vanadyl dimers.[50,51]

[1]Department of Materials, University of Oxford, Oxford OX1 3PH, UK

[2]Department of Chemistry, University of Oxford, Chemistry Research Laboratory, Oxford OX1 3TA, UK

[3]Electron-Spin Resonance Spectroscopy, Max Planck Institute for Multidisciplinary Sciences, Am Fassberg 11, 37077 Göttingen, Germany

[4]Department of Chemistry, Georg-August University of Göttingen, Tammannstr. 2, Göttingen, Germany

[5]National Crystallography Service, School of Chemistry, University of Southampton, Southampton SO17 1BJ, UK

[6]Centre for Advanced ESR, Department of Chemistry, University of Oxford, Inorganic Chemistry Laboratory, South Parks Road, Oxford OX1 3QR, UK

[7]These authors contributed equally

[8]Lead contact

*Correspondence:
iago.pozomiguez@chem.ox.ac.uk (I.P.),
lapo.bogani@materials.ox.ac.uk (L.B.),
harry.anderson@chem.ox.ac.uk (H.L.A.)

https://doi.org/10.1016/j.chempr.2023.09.013

Please cite this article in press as: Pozo et al., Enhanced coherence by coupling spins through a delocalized π-system: Vanadyl porphyrin dimers, Chem (2023), https://doi.org/10.1016/j.chempr.2023.09.013

Meso-aryl substituents are commonly used to tune the solubility of porphyrin polymers. *t*-Bu-substituted aryls are useful for growing crystals for X-ray diffraction analysis, whereas flexible side chains, such as $Si(C_6H_{13})_3$, confer higher solubility and prevent aggregation. Here, we test the effect of these solubilizing groups on the magnetic relaxation times of several different π-conjugated or non-conjugated porphyrin backbones. We show that porphyrin scaffolds can connect vanadyl centers without producing a drastic loss of coherence by investigating intermetallic interactions in dimers, as minimal models for synthetically accessible porphyrin arrays. These systems shed light on the relationship between the chemical structure and the relative strength of the magnetic interactions. They reveal how different substituents affect the phase memory time (T_m), providing insights into the structure-property relationships that govern the quantum performance of vanadyl porphyrin polymers.

In this article, we use rational codes to designate the porphyrin derivatives, as illustrated in Scheme 1. For example, in ***bl*-P2·VO^{THS}**, the prefix *bl* denotes "butadiyne linked," P2 indicates two porphyrins, VO signifies that the porphyrins are coordinated by vanadyl, and the super index THS specifies the side chain (THS, tri(*n*-hexyl)silyl; *t*-Bu, *tert*-butyl). When no solubilizing group is specified, we refer to compounds with both side chains. The other prefixes used for the porphyrin dimers are ethyne linked (*el*), singly linked (*sl*), syn-periplanar (*syn*), and anti-periplanar (*anti*).

RESULTS

Synthesis and chemical characterization

The vanadyl porphyrin monomers **P1·VO^{THS}** and **P1·VO^{tBu}** were prepared in almost quantitative yield by heating vanadyl acetylacetonate with the free-base porphyrins in phenol (Scheme 1).[6,52–54] We attempted to synthesize the alkyne-linked dimers ***bl*-P2·VO^{tBu}** and ***el*-P2·VO^{tBu}** from the corresponding free-base dimers under the same reaction conditions, but this resulted in decomposition; therefore, we inserted the vanadyl ion at an earlier stage in the synthesis (see supplemental information for the compounds containing THS and *t*-Bu groups, sections 1.2 and 1.3, respectively). Butadiyne-linked dimers (***bl*-P2·VO**) were obtained in high yields (>95%) by Pd-mediated Glaser coupling of ***Ph,e*-P1·VO** (Scheme 1). By contrast, the ethyne-linked dimers (***el*-P2·VO**) were synthesized in moderate yields by copper-free Sonogashira coupling, using triphenylarsine as ligand to avoid competing Glaser coupling.[55] The singly linked dimers ***sl*-P2·VO** were synthesized by direct insertion of vanadyl ions into the free-base dimers in 80% and 95% yields for the THS and *t*-Bu aryl substituted groups, respectively. The edge-fused dimers ***syn*-P2·VO^{THS}** and ***anti*-P2·VO^{THS}** were obtained in a 90% yield (4:5, *syn*:*anti*) from the corresponding free-bases by treatment with $VO(acac)_2$ in phenol at 180°C and separated by column chromatography on silica, with the *syn*-isomers being more polar (lower R_f). The analogous compounds ***syn*-P2·VO^{tBu}** and ***anti*-P2·VO^{tBu}** were prepared under the same reaction conditions. Full conversion was observed by thin-layer chromatography (TLC), but the yield of the two isomers was only 65% (1:1, *syn*:*anti*, separated by chromatography on SiO_2) due to their poor solubility in common organic solvents.

Single-crystal X-ray diffraction was used to determine the structures of **P1·VO^{THS}**, **P1·VO^{tBu}**, ***bl*-P2·VO^{tBu}**, ***el*-P2·VO^{tBu}**, ***sl*-P2·VO^{tBu}**, ***syn*-P2·VO^{tBu}**, and ***anti*-P2·VO^{tBu}** (Figure 2; supplemental information, section 5). In every structure, the asymmetric unit consists of one complete molecule, except for ***anti*-P2·VO^{tBu}**, in which case the asymmetric unit is half a porphyrin dimer. All these vanadyl porphyrins show V-O distances in the normal range for vanadyl porphyrins (1.56–1.64 Å), and the distances of the vanadium atoms from the plane of the porphyrin are in the range

Please cite this article in press as: Pozo et al., Enhanced coherence by coupling spins through a delocalized π-system: Vanadyl porphyrin dimers, Chem (2023), https://doi.org/10.1016/j.chempr.2023.09.013

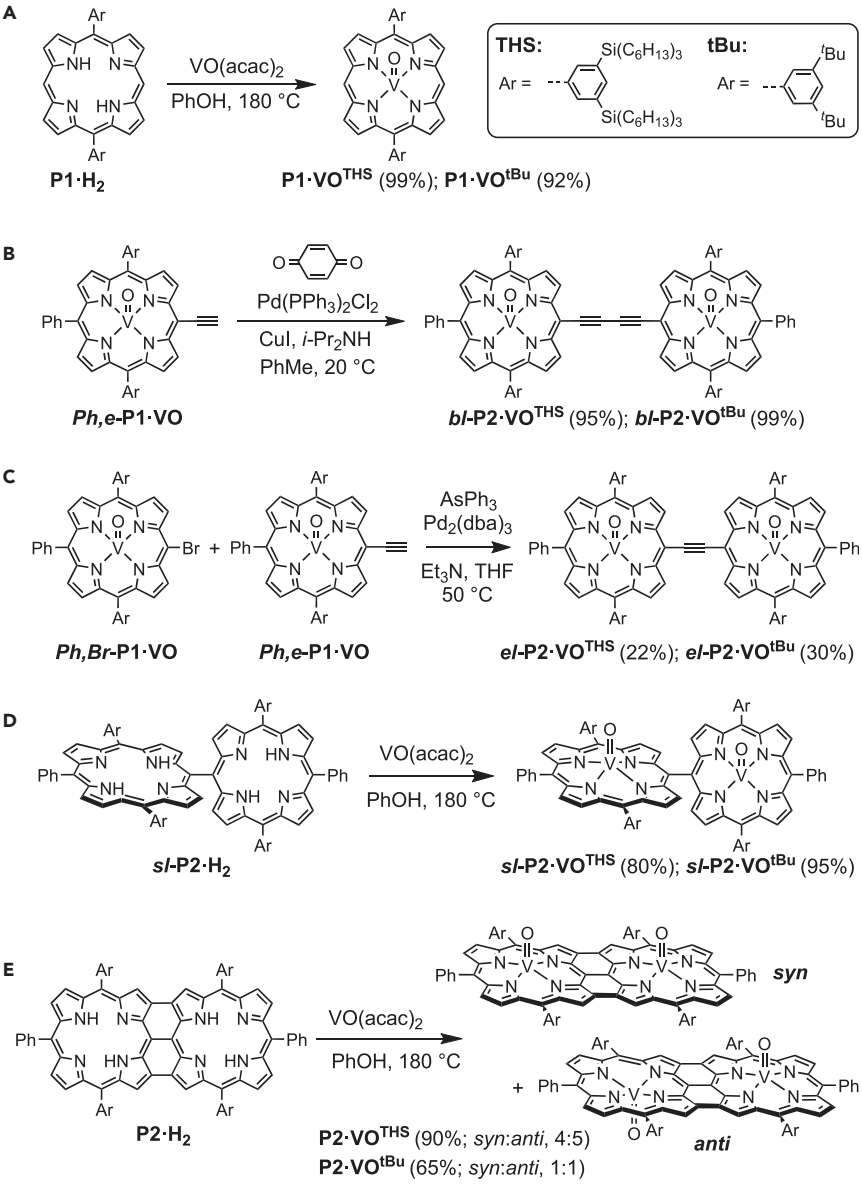

Scheme 1. Synthesis of vanadyl porphyrins

Synthesis of (A) P1·VO, (B) *bl*-P2·VO, (C) *el*-P2·VO, (D) *sl*-P2·VO, and (E) *syn*-P2·VO and *anti*-P2·VO, with the different side chains in the aryl substituted groups.

0.49–0.59 Å.[56–58] In general, flexible THS substituents prevent formation of suitable crystals for X-ray analysis; however, crystals of P1·VO^{THS} were grown by cooling a solution in acetamide. The intramolecular V···V distances in the dimers are as follows: *bl*-P2·VO^{tBu}, 13.367(1) Å; *el*-P2·VO^{tBu}, 10.896(1) Å; *sl*-P2·VO^{tBu}, 8.445(1) Å; *syn*-P2·VO^{tBu}, 8.402(6) Å; and *anti*-P2·VO^{tBu}, 8.466(3) Å. The alkyne-linked dimers *bl*-P2·VO^{tBu} and *el*-P2·VO^{tBu} crystallize in *syn*-periplanar conformations, with both vanadyl groups on the same face of the dimer. The angles between the planes of the porphyrins are 8.6° and 3.5° in *bl*-P2·VO^{tBu} and *el*-P2·VO^{tBu}, respectively. Coplanar conformations are often observed in crystal structures of butadiyne-linked[39] and ethyne-linked porphyrin dimers,[59,60] although a wide range of conformational angles is populated in solution.[61] The singly linked dimer *sl*-P2·VO^{tBu} has a

Please cite this article in press as: Pozo et al., Enhanced coherence by coupling spins through a delocalized π-system: Vanadyl porphyrin dimers, Chem (2023), https://doi.org/10.1016/j.chempr.2023.09.013

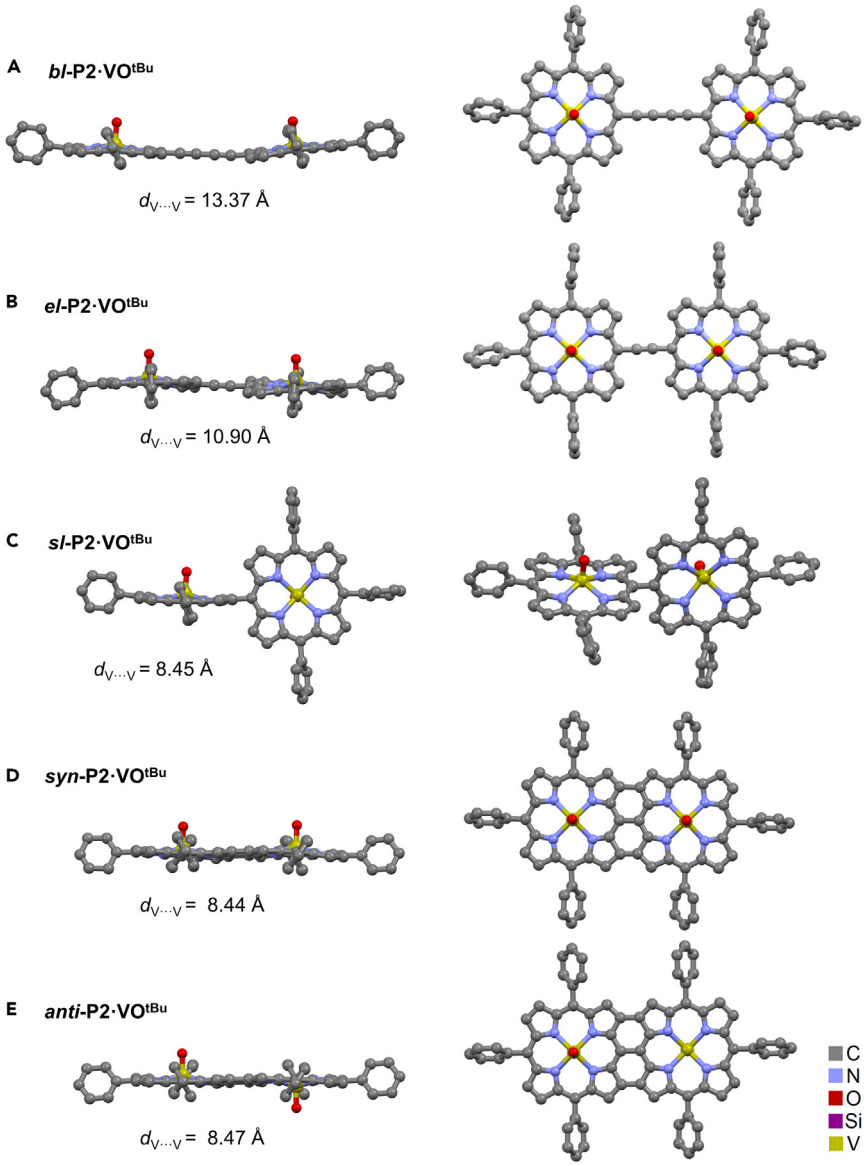

Figure 2. X-ray structure of vanadyl porphyrins

X-ray structure of *bl*-P2·VO^{tBu}, *el*-P2·VO^{tBu}, *sl*-P2·VO^{tBu}, *syn*-P2·VO^{tBu}, and *anti*-P2·VO^{tBu}. Hydrogens, *t*-Bu groups, and low-occupancy disordered atoms were omitted for clarity.

twisted conformation, as expected; the angle between the mean planes of the two porphyrin units is 83.4°. Recently, two polymorphs of a closely related singly linked vanadyl porphyrin dimer (Ar = Ph) were reported by Sorace and coworkers[51]; in these structures the angles between planes of the porphrins is 67.8° and 72.5°. The crystal structures of *syn*- and *anti*-P2·VO^{tBu} show disorder of the VO groups. In each case, the disorder could be modeled assuming the presence of just one isomer, and the sites of highest occupancy confirm the syn- and anti-stereochemistry. Both π-conjugated scaffolds are nearly planar; the root-mean-square deviation from planarity for the 48-atom cores are 0.10 Å for *syn*-P2·VO^{tBu} and 0.08 Å for *anti*-P2·VO^{tBu}.

The alkyne-linked dimers, *bl*-P2·VO^{tBu} and *el*-P2·VO^{tBu} form dimers-of-dimer π-π stacks in the solid state, suggesting a potential mode of aggregation in solution.

Please cite this article in press as: Pozo et al., Enhanced coherence by coupling spins through a delocalized π-system: Vanadyl porphyrin dimers, Chem (2023), https://doi.org/10.1016/j.chempr.2023.09.013

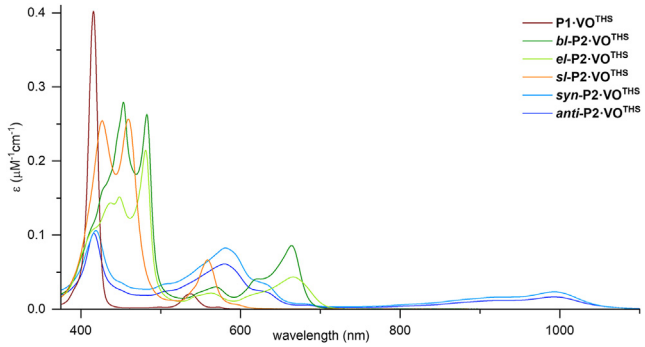

Figure 3. UV-vis-NIR spectra of vanadyl porphyrins

UV-vis-NIR absorption spectra of P1·VO^{THS}, *bl*-P2·VO^{THS}, *el*-P2·VO^{THS}, *sl*-P2·VO^{THS}, *syn*-P2·VO^{THS}, and *anti*-P2·VO^{THS} in dichloromethane at 25°C.

These bimolecular stacks are centrosymmetric, with the V=O units pointing outward, away from the center of the aggregate. The mean separation between the 48-atom porphyrin dimer planes in these stacks are 3.729 and 3.467 Å for *bl*-P2·VO^{tBu} and *el*-P2·VO^{tBu}, respectively. In both cases, the molecules are stacked in a parallel arrangement, offset along the alkyne axis, with interdigitated aryl side chains, as reported in related aggregates.[59,62] In the case of *el*-P2·VO^{tBu}, the center of one porphyrin sits directly above the central alkyne unit of the other dimer.

The ultraviolet-visible-near infrared (UV-vis-NIR) spectra of the THS-substituted compounds are shown in Figure 3. Changing the solubilizing group from THS to *t*-Bu has a negligible effect on the absorption spectra in dilute solution. The spectra of these vanadyl complexes are broadly similar to those of the corresponding porphyrin complexes of other first-row transition metals, such as Zn^{II}, Cu^{II}, or Ni^{II} (supplemental information, section 3). The absorption maxima are as follows: P1·VO, 414 and 536 nm[55]; *bl*-P2·VO, 453, 482, 619, and 662 nm[48]; *el*-P2·VO, 482 and 673 nm[55]; *sl*-P2·VO, 419, 456, and 558 nm[49]; and *syn*- and *anti*-P2·VO, 420, 580, and 995 nm.[40–44,49] Comparison of the lowest energy absorption bands shows that *el*-P2·VO is slightly more conjugated than *bl*-P2·VO and that both are more conjugated than *sl*-P2·VO. This observation was expected due to the almost perpendicular geometry of *sl*-P2·VO, as observed in the X-ray structure (Figure 2B). The absorption spectra of butadiyne- and ethyne-linked porphyrins reflect their flexible structures in solution,[37,61] beyond the approximately coplanar conformations in the crystalline states. The infrared (IR) spectra of all the vanadyl porphyrins exhibit intense peaks at around 1,004–1,009 cm^{-1} due to V=O bond stretching (supplemental information, section 3).

Magnetic properties

The continuous-wave electon paramagnetic resonance (CW-EPR) spectra of all the vanadyl porphyrins (except *syn*-P2·VO^{tBu} and *anti*-P2·VO^{tBu} due to their poor solubility) were recorded at X-band and Q-band (Figure 4; supplemental information, section 6) at 1 mM concentration in deuterated toluene frozen at 140 K. Pairs of compounds that differ only in the solubilizing group (THS vs. *t*-Bu) gave practically identical spectra, and they were simulated using the same parameters (collected in Table 1). Figure 4 shows the spectra of selected vanadyl porphyrins and their simulations (in black). The spectrum of P1·VO^{tBu} is similar to those of previously reported vanadyl porphyrin monomers,[63] with $g_{xy} = 1.984 \pm 0.008$ and $g_z = 1.961 \pm 0.007$ for in- and off-plane contributions,[64] and anisotropic hyperfine coupling, ***A***,[65,66] to the ^{51}V nucleus ($I = 7/2$) with $A_{xy} = 170$ MHz and $A_z = 477$ MHz.

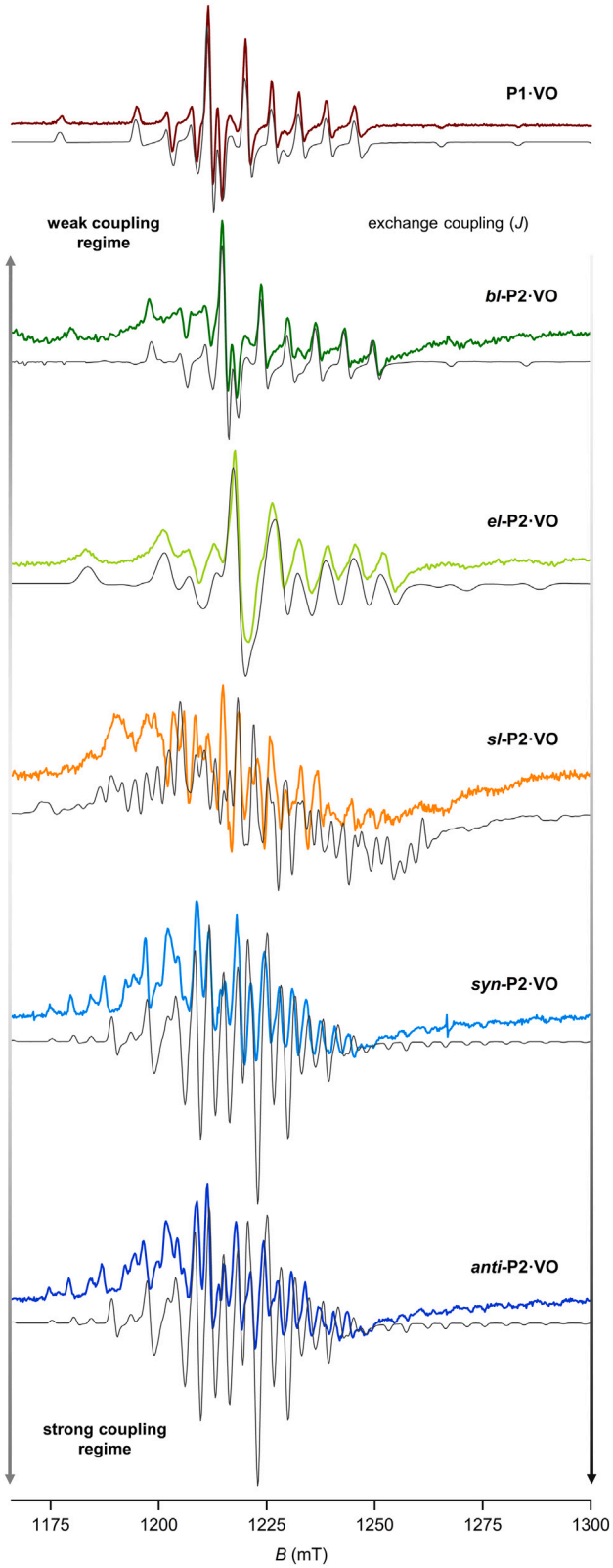
P1·VO
weak coupling regime
exchange coupling (J)
bl-P2·VO
el-P2·VO
sl-P2·VO
syn-P2·VO
anti-P2·VO
strong coupling regime
1175
1200
1225
1250
1275
1300
B (mT)

Figure 4. Q-band CW-EPR spectra of vanadyl porphyrins

CW-EPR spectra of P1·VO^{tBu}, *bl*-P2·VO^{tBu}, *el*-P2·VO^{tBu}, *sl*-P2·VO^{tBu}, *syn*-P2·VO^{THS}, and *anti*-P2·VO^{THS}. Simulations are shown in black. All spectra recorded at 140 K at 33.9 GHz in frozen deuterated toluene solutions (1 mM). EPR parameters used for the simulations are listed in Table 1.

Simulation of the spectra of the dimers was achieved with the Hamiltonian:

$$H = \mu_B \sum_{i=1}^{2} \boldsymbol{B} \boldsymbol{g}_i \hat{\boldsymbol{S}}_i + \sum_{k,j=1,2} \hat{\boldsymbol{S}}^k \boldsymbol{A}^j \hat{\boldsymbol{I}} + \hat{S}_1 D \hat{S}_2 + \hat{S}_1 J \hat{S}_2 \qquad \text{(Equation 1)}$$

where μ_B is the Bohr magneton, $\boldsymbol{B}$ is the external magnetic field, $\hat{\boldsymbol{S}}$ and $\hat{\boldsymbol{I}}$ are the electron and nucleus spin operators. The alkyne-linked dimers ***bl*-P2·VO** and ***el*-P2·VO** present similar EPR spectra with $\boldsymbol{g}$ and $\boldsymbol{A}$ values g_{xy} = 1.984 ± 0.008 and g_z = 1.96 1 ± 0.007, A_{xy} = 170 ± 4 MHz and A_z = 477 ± 8 MHz, close to those observed for the monomer (Table 1; Figure 4). The major differences arise from the small effect of exchange and dipolar interactions (***bl*-P2·VO**: D = 10.74 ± 0.25 MHz, J = 9.97 ± 0.23 MHz; and ***el*-P2·VO**: D = 14.67 ± 0.34 MHz, J = 13.07 ± 0.30 MHz, antiferromagnetic coupling). The singly linked dimers ***sl*-P2·VO** are in an intermediate situation, not being weakly interacting doublets nor pure triplets, as recently reported for an analogous molecule.[51] The best simulation was achieved assuming the behavior as two weakly interacting doublets with the following set of parameters: g_{xy} = 1.984 ± 0.008 and g_z = 1.961 ± 0.007, A_{xy} = 170 ± 4 MHz and A_z = 477 ± 8 MHz, D = 84 ± 2 MHz, and J = 272 ± 6 MHz, with antiferromagnetic coupling. The values obtained in this way are in good agreement with those reported for a magnetically equivalent system.[51]

The Landé factors g_{xy} = 1.987 ± 0.008 and g_z = 1.964 ± 0.007 of ***anti*-P2·VO^{THS}** and ***syn*-P2·VO^{THS}** are similar to those of **P1·VO^{THS}**, confirming that the much more complex EPR spectra of these dimers can be interpretated in terms of two coupled monomers. The splitting produced by the hyperfine coupling drastically depends on the exchange regime.[66] If the strongest interaction is the hyperfine coupling rather than the exchange interaction ($A >> J$), then the overall spectral shape follows that for a typical vanadyl porphyrin monomer, such as **P1·VO^{THS}**, as is the case for ***bl*-P2·VO** and ***el*-P2·VO**, and previously reported vanadyl dimers.[67,68] On the other hand, if exchange coupling dominates ($J >> A$), the unpaired electrons interact equally with both nuclear spins. In this case, the spectrum is expected to display halved A values[66,69–71] and two sets of hyperfine splitting, with 15 lines each ($2NI + 1$, where N = 2 and I = 7/2) with higher intensities in the center and distortions from other interactions, such as dipolar coupling, as discussed below. The resulting patterns can be extremely complex, and simulating these spectra can be highly informative. The spectra recoded for ***syn*-P2·VO^{THS}** and ***anti*-P2·VO^{THS}** indicate that they are in an intermediate-exchange regime dominated by the J

Table 1. EPR parameters for vanadyl porphyrins from simulation of Q-band spectra[a]

	P1·VO	*bl*-P2·VO	*el*-P2·VO	*sl*-P2·VO	*syn*-P2·VO[b]	*anti*-P2·VO[b]
Spin	½	S1 = ½, S2 = ½	S1 = ½, S2 = ½	S1 = ½, S2 = ½	1	1
g_{xy}	1.984 ± 0.008	1.984 ± 0.008	1.984 ± 0.008	1.984 ± 0.008	1.987 ± 0.008	1.987 ± 0.008
g_z	1.961 ± 0.007	1.961 ± 0.007	1.961 ± 0.007	1.961 ± 0.007	1.964 ± 0.007	1.964 ± 0.007
A_{xy} (MHz)	170 ± 4	170 ± 4	170 ± 4	170 ± 4	85.3 ± 2.0	85.3 ± 2.0
A_z (MHz)	477 ± 8	477 ± 8	477 ± 8	477 ± 8	261.6 ± 4.4	261.6 ± 4.4
D (MHz)	–	10.74 ± 0.25	14.67 ± 0.34	84 ± 2	186 ± 4.3	186 ± 4.3
J (MHz)	–	9.97 ± 0.23	13.07 ± 0.30	272 ± 6	2350 ± 54	2350 ± 54

[a] g, Landé factor; A, hyperfine coupling; J, exchange coupling; D, dipolar coupling. All five dimers exhibit antiferromagnetic coupling.
[b] J was not included in the simulation of EPR spectra of ***syn*-P2·VO** and ***anti*-P2·VO** at Q-band. J values were obtained from EPR spectra at the J-band (Figure 5).

Please cite this article in press as: Pozo et al., Enhanced coherence by coupling spins through a delocalized π-system: Vanadyl porphyrin dimers, Chem (2023), https://doi.org/10.1016/j.chempr.2023.09.013

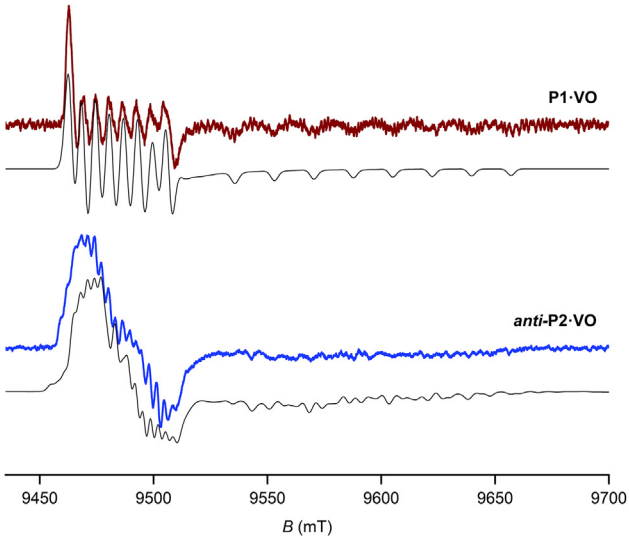

Figure 5. J-band EPR spectra of vanadyl porphyrins

First derivative, pseudo-modulated ESE spectra of **P1·VO**^{THS} and ***anti*-P2·VO**^{THS}. Simulations are shown in black. Spectra were recorded at 10 K at 263 GHz in frozen deuterated toluene solutions (5 mM). The simulation for ***anti*-P2·VO**^{THS} was calculated with an exchange coupling of J = 2.35 GHz, together with the other parameters listed in Table 1. Amplitude for pseudo-modulation was 2 mT.

interaction ($J > A$), as also confirmed by the J-band experiments that yield $J \approx 2.35$ GHz (see below). This places the conjugated vanadyl dimers in a scenario that is different from previous non-conjugated molecular architectures,[51,67,68] which are paired quantum mechanically by dominant hyperfine and dipole-dipole interactions, rather than exchange coupling. Simulation of the Q-band spectra was performed using the Hamiltonian in Equation 1, considering a dominant J contribution and the hyperfine coupling values roughly half those of the monomer, to create two overlapping hyperfine patterns of 15 lines with constants $A^1_{xy} = A^2_{xy} = 261.6 \pm 4.4$ MHz, $A^1_z = A^2_z = 85.3 \pm 2.0$ MHz centered at $g_{xy} = 1.987 \pm 0.008$ and $g_z = 1.964 \pm 0.007$, respectively, and further split by $D = 186 \pm 4$ MHz; see simulated spectra (black) in Figure 4. This experimental value of D can be compared with the calculated value obtained using the point-dipole approximation (this model is known to underestimate D for a determined distance),[72] leading to values of 128 and 131 MHz for the distances of 8.400 and 8.465 Å, in good agreement with our simulation. The broad features underlying the spectra may be attributed to J anisotropy.[69–71]

In order to extract more information from the complex pattern produced in the intermediate coupling regimes, we recorded electron spin echo (ESE)-detected EPR spectra of **P1·VO**^{THS} and ***anti*-P2·VO**^{THS} at higher frequency and fields (J-band, 263 GHz). The resulting first derivative, pseudo-modulated ESE spectra are presented in Figure 5. At this field, the perpendicular (xy) and parallel (z) transitions are well separated at 9,450–9,520 and 9,530–9,670 mT, respectively. Excellent agreement was obtained, by simulating the spectrum of ***anti*-P2·VO**^{THS} using a model that describes the system as two unpaired electrons (2x S = ½) that interact with each other through D and J couplings and with their respective V^{IV} nucleus (S = 7/2). Landé factors and dipolar coupling were equivalent to those used in the Q-band simulation (above), but non-halved hyperfine interactions are used in this case (A_{xy} = 170 and A_z = 477 MHz). The best simulation was achieved with antiferromagnetic J = 2,350 ± 54 MHz, which shows that the system is near the strong

Please cite this article in press as: Pozo et al., Enhanced coherence by coupling spins through a delocalized π-system: Vanadyl porphyrin dimers, Chem (2023), https://doi.org/10.1016/j.chempr.2023.09.013

coupling regime. These exchange-coupling values are much larger than in previously reported bis-vanadyl complexes with similar inter-spin distances[51,67,68] but two orders of magnitude weaker than in the analogous Cu(II) porphyrin dimer.[45,46] Acceptable agreement could not be obtained with smaller J values but was also observed with larger J values (supplemental information, section 6). However, values of J larger than 3 GHz would not be consistent with the results from superconducting quantum interference device (SQUID) magnetometry (discussed below). Because the Q-band spectra of ***syn***- and ***anti***-P2·VO^{THS} are almost identical (Figure 4), we assume that both isomers present similar exchange coupling of $J \approx 2.35$ GHz.

We also investigated ***syn***-P2·VO^{THS} and ***anti***-P2·VO^{THS} using SQUID magnetometry. The exchange coupling is too small to be determined reliably by this technique, but these experiments provided an upper limit of $J \leq 3$ GHz and gave information about the number of unpaired electrons per molecule (supplemental information, section 7). The molar magnetic susceptibilities of the dimers ***syn***-P2·VO^{THS} and ***anti***-P2·VO^{THS} at room temperature (T = 300 K; $\chi_M T$ = 0.732 and 0.731 emu K mol^{-1}, respectively) are in agreement with the expected value for two unpaired electrons (0.750 emu K mol^{-1}) and approximately twice the value of the monomer P1·VO^{THS} (0.372 emu K mol^{-1}) (see supplemental information for more details of SQUID magnetometry studies, section 7, Figures S111–S119).[73] When $H >> kT$, the magnetization saturates at around 2 $N\mu_B$, as the expected for a spin triplet (S = 1) or two doublets (2x S = ½).[73]

Density functional theory (DFT) calculations gave S-T gaps the for the porphyrin dimers (without *t*-Bu or THS chains, geometries in the supplemental information) that reproduce the trend in the experimental J values, although the predicted gaps for ***bl***-P2·VO and ***el***-P2·VO are substantially larger than the experimental values (see supplemental information for details, section 8, Table S3). Calculations for ***anti***-P2·VO using a range of functionals (DFT-B3LYP, PBE0, and CAM B3LYP with the 6-31G** basis set) predicted J values in the range of 2.7–4.5 GHz.

Q-band pulsed electron paramagnetic resonance

The quantum behavior of the vanadyl porphyrins was studied by pulse EPR. The spin-lattice relaxation time (T_1) was determined by fitting the Picket-Fence recovery traces with a bi-exponential model (Figure 6B, see supplemental information for more details, section 6.1), yielding values on the order of milliseconds for the selected vanadyl porphyrins (P1·VO^{THS}, ***bl***-P2·VO^{tBu}, ***el***-P2·VO^{tBu}, ***sl***-P2·VO^{tBu}, ***syn***-P2·VO^{THS}, and ***anti***-P2·VO^{THS}). The temperature dependence of T_1^{-1} reveals similar phonon-mediated relaxation processes for all the compounds: direct processes below 20 K and Raman processes between 20 and 80 K, as reported for other V(IV) complexes (supplemental information, section 6, Figure S64).[10]

Spin phase memory times

The phase memory times (T_m) were determined using a Hahn echo sequence (Figure 6A), fitting echo decay traces (e.g., Figure 6C) with a stretched exponential model (supplemental information, section 6). T_m values of vanadyl porphyrin dimers containing THS chains are shown in Figure 6D. The five vanadyl pairs exhibit increasing T_m values with decreasing temperature (80–20 K). The dimers in the weakly coupled (***bl***-P2·VO^{THS}, ***el***-P2·VO^{THS}, and ***sl***-P2·VO^{THS}) reach a maximum between 10 and 20 K and suffer a pronounced drop of T_m on lowering the temperature (below 10 K). Surprisingly, ***syn***-P2·VO^{THS} and ***anti***-P2·VO^{THS} isomers display a different behavior, increasing continuously from 80 K with maximum values at 4 K (4.6 and 5.2 μs, respectively). Apparently, the dominant exchange coupling via a

Please cite this article in press as: Pozo et al., Enhanced coherence by coupling spins through a delocalized π-system: Vanadyl porphyrin dimers, Chem (2023), https://doi.org/10.1016/j.chempr.2023.09.013

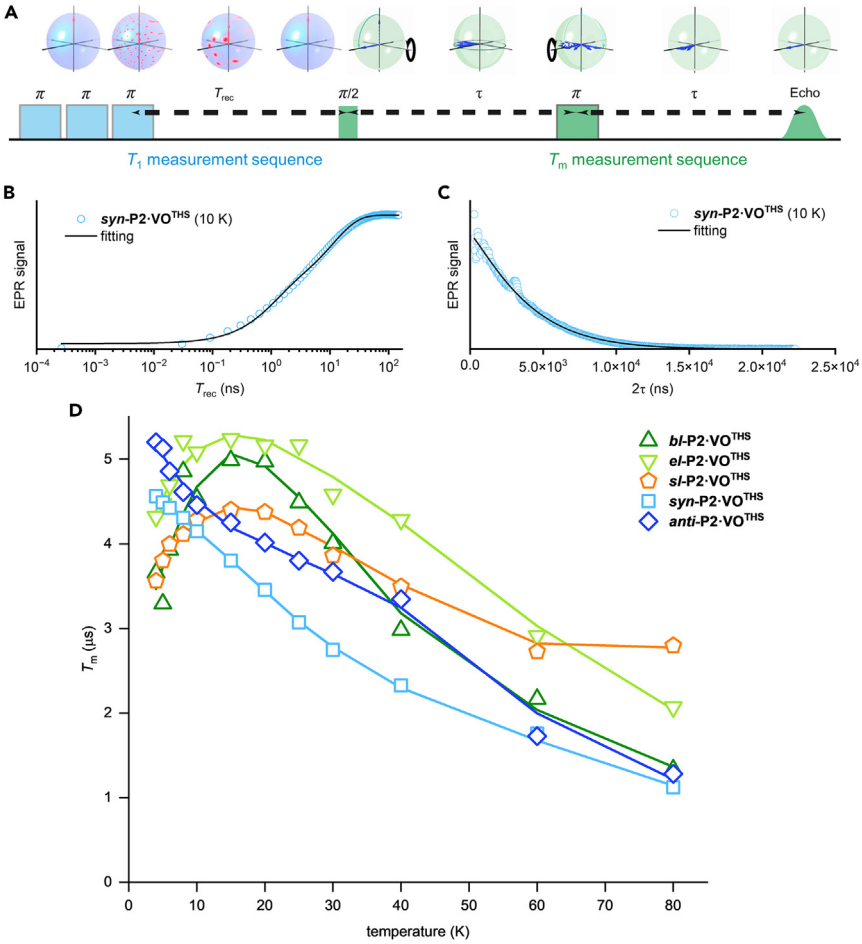

Figure 6. Spin-spin and spin-lattice relaxation times

(A) Pulse sequences used to measure the characteristic relaxation times and Bloch sphere depiction.

(B) Picket-Fence recovery trace and a fit with a bi-exponential function (black line, discussed in the supplemental information) of ***syn*-P2·VO^{THS}** at 10 K.

(C) The Hahn echo decay trace and a fit with a stretched exponential function of ***syn*-P2·VO^{THS}** at 10 K.

(D) Temperature dependence of the phase memory times (T_m) of vanadyl dimers containing THS (solid trend lines are included as visual guide). All measurements at Q-band, at 33.9 GHz, and in frozen deuterated toluene solutions (1 mM).

delocalized channel leads to suppression of decoherence at low temperatures (<10 K), as previously observed in Si quantum dots and Ti atoms.[17–21] This behavior has not been reported previously for molecular systems and may be attributed to the strong π-conjugation in ***syn***- and ***anti*-P2·VO^{THS}**.

At low temperatures, the phase memory time (T_m) can be affected by small-angle molecular motions in glassy organic solvents (librations)[74] and spin-spin interactions.[15] We studied the *t*-Bu-substituted dimers, ***bl*-P2·VO^{tBu}**, ***el*-P2·VO^{tBu}**, and ***sl*-P2·VO^{tBu}**, which exhibited the same pronounced coherence drop below 10 K as the corresponding THS-containing analogs (Figure S63B). Compounds containing THS chains are more flexible and practically double the molecular weight of those containing *t*-Bu groups; hence, libration movements in these systems are less probable, and it is unlikely that both families of compounds (THS and *t*-Bu) will be equally affected by this type of relaxation. Intramolecular spin-spin interactions due to

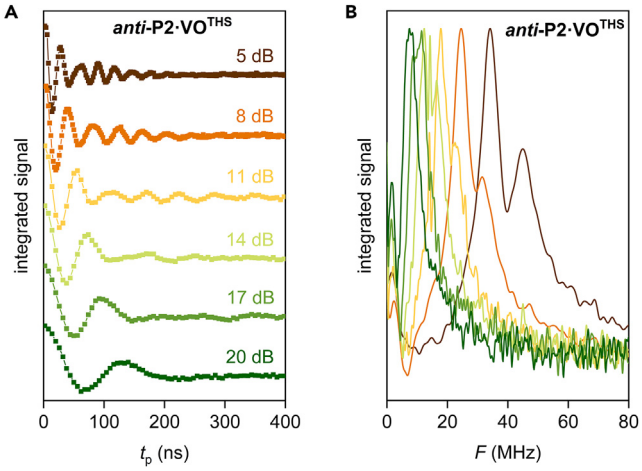

Figure 7. Transient nutation experiments

(A) Rabi oscillations at different power attenuation, ***anti*-P2·VO^{THS}**, T = 10 K, ν = 9.5 GHz.

(B) Fourier transform of the oscillation.

hyperfine couplings are not expected to be significantly different in the two families of compounds because the H nuclei on the porphyrin backbones are practically the same for all the systems and within spin-diffusion barrier.[7,10,15] The H nuclei in the THS chains seem to produce 1–2 μs lower T_m values than the analogous compounds with *t*-Bu substituents across the whole temperature range (Figures S63A and S63B). For these reasons, the coherence loss below 10 K of the weakly coupled compounds can be attributed to the electron pair flip-flops.[15] Importantly, this effect is not relevant in ***syn***- and ***anti*-P2·VO^{THS}**, demonstrating that the presence of a dominant exchange interaction (*J*) leads to the suppression of decoherence. Furthermore, the dominant exchange coupling is inevitably related with the presence of the π-delocalized backbone, allowing us to establish a clear relationship between chemical structure, magnetic interactions, and quantum coherence: strong π-conjugation/dominant exchange coupling/longer T_m (below 10 K).

The study of Rabi oscillations was used to investigate whether the system can be placed in a quantum superposition and reveal other potential decoherence channels. Transient nutation experiments were performed for selected vanadyl porphyrins (***bl*-P2·VO^{tBu}**, ***el*-P2·VO^{tBu}**, ***sl*-P2·VO^{tBu}**, ***syn*-P2·VO^{THS}**, and ***anti*-P2·VO^{THS}**) yielding similar results (supplemental information, section 6). Figure 7 shows the Rabi oscillations for ***anti*-P2·VO^{THS}**. Their Fourier transform show linear B_1 dependance of the Rabi frequency of the main peaks and does not present any constant feature. This observation indicates that the hyperfine couplings (e.g., with the peripheral hydrogens) do not introduce alternative decoherence pathways to those previously mentioned in this article (phonon-mediated processes; direct and Raman, and electron pair flip-flops).

DISCUSSION

The spin-density maps, calculated with DFT, B3LYP6-31G(d,p) show that the unpaired electrons are located in $3d_{xy}$ orbitals of the vanadium atoms, as previously reported for vanadyl porphyrins[63] and as expected for a d^1 configuration (Figure 8).[75] The d_{xy} orbital is aligned between the nitrogen atoms of the porphyrin core, minimizing interactions of the unpaired spin with the porphyrin or with the environment, which favors a long phase memory time[7] and a relatively weak exchange coupling. The stronger exchange coupling in the analogous Cu(II) porphyrins arises because

Please cite this article in press as: Pozo et al., Enhanced coherence by coupling spins through a delocalized π-system: Vanadyl porphyrin dimers, Chem (2023), https://doi.org/10.1016/j.chempr.2023.09.013

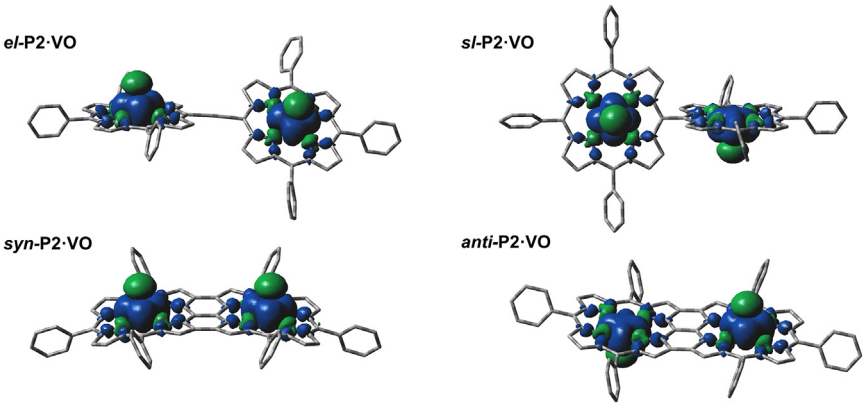

Figure 8. Spin-density surfaces
Spin-density surfaces of ***el***-P2·VO, ***sl***-P2·VO, ***syn***-P2·VO, and ***anti***-P2·VO.

in that case the d^9 configuration places the unpaired spin in a $d_{x^2-y^2}$ orbital, which has a direct interaction with the nitrogen atoms and thus with the π-systems.[45,46]

Counterintuitively, ***sl***-P2·VO dimers have a stronger exchange interaction (J = 272 MHz) than the π-conjugated alkyne-linked dimers ***bl***-P2·VO and ***el***-P2·VO (J = 10 and 13 MHz, respectively, from the CW-EPR simulations), which implies that significant exchange interaction occurs through the σ-bond and that the shorter metal-metal distance in ***sl***-P2·VO compensates for its lack of π-conjugation. However, in the strongly conjugated systems, which have similar V···V distances, ***syn***- and ***anti***-P2·VO, the exchange coupling is drastically increased, surpassing the strength of the hyperfine coupling and placing these compounds in the J-dominated regime. The structural and magnetic analysis of the molecules is crucial to study their quantum performance.[76,77] Although weakly coupled compounds have similar trends, with maxima values of phase memory time (T_m) at 10–20 K, the compounds dominated by the exchange coupling (J) exhibit a continuous increase in phase memory time with decreasing the temperature. Comparison between magnetically equivalent compounds with different substituents is essential for identifying the main decoherence pathways at different temperatures. This analysis indicates that the different trends below 10 K are related to electron spin flip-flop processes, which are one of the most relevant sources of decoherence in solid materials. These observations indicate that exchange coupling can be used to suppress the decoherence originating from this process in molecular spin systems.

Conjugated quantum mediators can transport electrons in conduction channels while preserving magnetic information and be operated on chip by applying magnetic fields or microwaves.[78–87] When considering recent results on fused[40–43,88] and magnetic porphyrins,[10,45–49,89] together with the chemical structure/quantum coherence relationships reported in this article, these results demonstrate the suitability of magnetic porphyrin materials for quantum applications; the integration into single-electron transistors seems practicable, with the perspective to create molecular systems that can be used in single-molecule devices with magnetic control and electrical readout and with potential applications in quantum information processing, as spin valves or spin filters.[30,86–91] The suppression of decoherence at low temperatures by molecular design is crucial because the magnetic states are very close in energy (usually <1 meV); thus, their electrical readout is necessarily available only at temperatures below 10 K.[92,93] With that regard, extended materials

Please cite this article in press as: Pozo et al., Enhanced coherence by coupling spins through a delocalized π-system: Vanadyl porphyrin dimers, Chem (2023), https://doi.org/10.1016/j.chempr.2023.09.013

based on P2·VO might offer an interesting platform, having a conduction channel available while keeping long phase memory times at low temperatures. These results constitute a fundamental step for the development of spin-electronic molecular quantum units.

Conclusions

We report the synthesis of 12 vanadyl porphyrins; two monomeric systems and ten dimers. The characterization of these compounds was performed by standard methods (e.g., mass spectrometry, IR, and UV-vis-NIR spectroscopy), accurate structural information was achieved by X-ray diffraction analysis, and their π-conjugation was probed by UV-vis-NIR spectroscopy. CW-EPR spectra show that dimers ***bl***-P2·VO and ***el***-P2·VO behave as two weakly interacting vanadyl centers ($J/A \approx 0.03$). Compounds ***sl***-P2·VO present a mixed spin state, as recently reported for an analogous compound,[51] with a relatively high exchange coupling ($J/A \approx 0.6$) despite the lack of π-conjugation, which indicates significant exchange coupling through the σ-bond between *meso-meso*-linked porphyrins. In contrast, ***syn***- and ***anti***-P2·VO are strongly π-conjugated with efficient electron-electron communication through the multiply connected π-system, with an intermetallic distance of 8.4–8.5 Å. The combined use of EPR spectroscopy at Q- and J-bands allowed us to quantify the magnetic interactions in these systems, describing for the first-time vanadyl pairs in the *J*-dominated regime ($J/A \approx 5$).

These systems all exhibit spin-lattice relaxation times (T_1) in the millisecond range with similar phonon-mediated decoherence pathways. The study of the phase memory time (T_m) at different temperatures shows that the compounds weakly coupled (***bl***-P2·VO, ***el***-P2·VO, and ***sl***-P2·VO) have a coherence drop below 10 K, whereas the compounds in the exchange dominated regime (***syn***- and ***anti***-P2·VO) exhibit increasing T_m with decreasing temperature. This difference is attributed to the influence of electron pair flip-flop processes by comparing magnetically equivalent systems with different substituents (THS and *t*-Bu). The immersion of vanadyl units in a strongly π-conjugated scaffold places the systems in the *J*-dominated regime, increasing their exchange interaction and protecting the phase memory time, as previously observed in non-molecular systems. The use of 2D electron gases to connect spins without suppressing their coherence has been observed in surface nanostructures made of semiconductors,[94–97] and the origins of this effect remain subject to debate.[98,99] Our observation of this effect at the molecular scale can now prompt a rigorous theoretical analysis, in systems where every atomic position is known and that can be modeled in detail. We thus expect these results to impact not only the synthetic community but also the theoreticians working on quantum systems.

These results show that the chemistry of porphyrin polymers can be used to create conducting molecular materials with multiple quantum units linked together, tuning the spin-spin couplings in a rational manner, which are in the range of suitable values for quantum information processing. We demonstrate that the use of a conjugated backbone produces multiple spin centers that communicate efficiently but do not suffer from decoherence issues that traditionally plague interacting quantum systems. This combination of features is appealing for the design of functional magnetic materials for single-molecule devices. Having multiple spins that interact coherently is the first step in creating molecular devices where quantum operations can be performed. The systems presented here can be integrated into molecular junction devices[100,101] where the spin levels can be read electrically.[90] They thus offer an excellent platform for the full control of molecular systems in transport devices, controlled by microwave irradiation at low temperatures.

Please cite this article in press as: Pozo et al., Enhanced coherence by coupling spins through a delocalized π-system: Vanadyl porphyrin dimers, Chem (2023), https://doi.org/10.1016/j.chempr.2023.09.013

EXPERIMENTAL PROCEDURES

Resource availability

Lead contact

Further information and requests for resources should be directed to and will be fulfilled by the lead contact, Harry Anderson (harry.anderson@chem.ox.ac.uk).

Materials availability

The materials generated are available from the lead contact upon reasonable request.

Data and code availability

The accession number for compounds P1·VO^{THS}, P1·VO^{tBu}, *bl*-P2·VO^{tBu}, *el*-P2·VO^{tBu}, *sl*-P2·VO^{tBu}, *anti*-P2·VO^{tBu}, and *syn*-P2·VO^{tBu} reported in this paper are CCDC: 2195114, 2252300, 2252302, 2252301, 2252303, 2195115, and 2195116, respectively.

All data supporting the conclusions of this study are available in the main text and supplemental information or from the lead contact upon reasonable request.

SUPPLEMENTAL INFORMATION

Supplemental information can be found online at https://doi.org/10.1016/j.chempr.2023.09.013.

ACKNOWLEDGMENTS

We thank the EPSRC (grant nos. EP/R029229/1 and EP/R042594/1), the Royal Society (URF and grant), the European Union (ERC-CoG-773048-MMGNR and ERC-ADG 885606 ARO-MAT), and the Margarita Salas Postdoctoral Fellowship (Next Generation EU, Gobierno de España – Ministerio de Universidades) for financial support. We thank the EPSRC UK National Crystallography Service at the University of Southampton for the collection of crystallographic data.

AUTHOR CONTRIBUTIONS

I.P., L.B., and H.L.A. conceived the project. Z.H., F.L., and M.S. carried out the X-band and Q-band EPR measurements, analysis, and simulations. I.T. and M.B. carried out the J-band EPR measurements. I.T., I.P., L.B., W.K.M., and Z.H. carried out the J-band EPR analysis and simulations. W.K.M. provided assistance and support with the EPR experiments. I.P. and J.-R.D. conducted the synthesis and chemical characterization. I.P. and F.K. performed the theoretical calculations. D.I.A. carried out SQUID magnetometry. W.S., P.N.H., and S.J.C. performed X-ray crystallography. I.P., L.B., and H.L.A. coordinated and supervised the project. All authors contributed to the manuscript.

DECLARATION OF INTERESTS

The authors declare no competing interests.

INCLUSION AND DIVERSITY

We support inclusive, diverse, and equitable conduct of research.

Received: April 5, 2023
Revised: August 13, 2023
Accepted: September 18, 2023
Published: October 11, 2023

REFERENCES

1. Zadrozny, J.M., Niklas, J., Poluektov, O.G., and Freedman, D.E. (2014). Multiple quantum coherences from hyperfine transitions in a vanadium(IV) complex. J. Am. Chem. Soc. *136*, 15841–15844. https://doi.org/10.1021/ja507846k.

2. Zadrozny, J.M., Niklas, J., Poluektov, O.G., and Freedman, D.E. (2015). Millisecond coherence time in a tunable molecular electronic spin Qubit. ACS Cent. Sci. *1*, 488–492. https://doi.org/10.1021/acscentsci.5b00338.

3. Graham, M.J., Krzyaniak, M.D., Wasielewski, M.R., and Freedman, D.E. (2017). Probing nuclear spin effects on electronic spin coherence via EPR measurements of vanadium(IV) complexes. Inorg. Chem. *56*, 8106–8113. https://doi.org/10.1021/acs.inorgchem.7b00794.

4. Jain, S.K., Yu, C.-J., Wilson, C.B., Tabassum, T., Freedman, D.E., and Han, S. (2021). Dynamic nuclear polarization with vanadium(IV) metal centers. Chem *7*, 421–435. https://doi.org/10.1016/j.chempr.2020.10.021.

5. Atzori, M., Morra, E., Tesi, L., Albino, A., Chiesa, M., Sorace, L., and Sessoli, R. (2016). Quantum coherence times enhancement in vanadium(IV)-based potential molecular qubits: the key role of the vanadyl moiety. J. Am. Chem. Soc. *138*, 11234–11244. https://doi.org/10.1021/jacs.6b05574.

6. Yamabayashi, T., Atzori, M., Tesi, L., Cosquer, G., Santanni, F., Boulon, M.E., Morra, E., Benci, S., Torre, R., Chiesa, M., et al. (2018). Scaling up electronic spin qubits into a three-dimensional metal–organic framework. J. Am. Chem. Soc. *140*, 12090–12101. https://doi.org/10.1021/jacs.8b06733.

7. Graham, M.J., Yu, C.J., Krzyaniak, M.D., Wasielewski, M.R., and Freedman, D.E. (2017). Synthetic approach to determine the effect of nuclear spin distance on electronic spin decoherence. J. Am. Chem. Soc. *139*, 3196–3201. https://doi.org/10.1021/jacs.6b13030.

8. Tesi, L., Lucaccini, E., Cimatti, I., Perfetti, M., Mannini, M., Atzori, M., Morra, E., Chiesa, M., Caneschi, A., Sorace, L., and Sessoli, R. (2016). Quantum coherence in a processable vanadyl complex: new tools for the search of molecular spin qubits. Chem. Sci. *7*, 2074–2083. https://doi.org/10.1039/C5SC04295J.

9. Moreno-Pineda, E., Godfrin, C., Balestro, F., Wernsdorfer, W., and Ruben, M. (2018). Molecular spin qudits for quantum algorithms. Chem. Soc. Rev. *47*, 501–513. https://doi.org/10.1039/C5CS00933B.

10. Yu, C.J., Graham, M.J., Zadrozny, J.M., Niklas, J., Krzyaniak, M.D., Wasielewski, M.R., Poluektov, O.G., and Freedman, D.E. (2016). Long coherence times in nuclear spin-free vanadyl qubits. J. Am. Chem. Soc. *138*, 14678–14685. https://doi.org/10.1021/jacs.6b08467.

11. Gimeno, I., Urtizberea, A., Román-Roche, J., Zueco, D., Camón, A., Alonso, P.J., Roubeau, O., and Luis, F. (2021). Broad-band spectroscopy of a vanadyl porphyrin: a model electronuclear spin qudit. Chem. Sci. *12*, 5621–5630. https://doi.org/10.1039/D1SC00564B.

12. Jiang, S., Goß, K., Cervetti, C., and Bogani, L. (2012). An introduction to molecular spintronics. Sci. China Chem. *55*, 867–882. https://doi.org/10.1007/s11426-012-4628-4.

13. Cornia, A., and Seneor, P. (2017). Spintronics: the molecular way. Nat. Mater. *16*, 505–506. https://doi.org/10.1038/nmat4900.

14. Gaita-Ariño, A., Luis, F., Hill, S., and Coronado, E. (2019). Molecular spins for quantum computation. Nat. Chem. *11*, 301–309. https://doi.org/10.1038/s41557-019-0232-y.

15. Mirzoyan, R., Kazmierczak, N.P., and Hadt, R.G. (2021). Deconvolving contributions to decoherence in molecular electron spin qubits: a dynamic ligand field approach. Chemistry *27*, 9482–9494. https://doi.org/10.1002/chem.202100845.

16. Huang, P. (2021). Dephasing of exchange-coupled spins in quantum dots for quantum computing. Adv. Quantum Technol. *4*, 2100018. https://doi.org/10.1002/qute.202100018.

17. Li, Q., Cywiński, Ł., Culcer, D., Hu, X., and Das Sarma, S. (2010). Exchange coupling in silicon quantum dots: theoretical considerations for quantum computation. Phys. Rev. B *81*, 085313. https://doi.org/10.1103/PhysRevB.81.085313.

18. De, A., Lang, A., Zhou, D., and Joynt, R. (2011). Suppression of decoherence and disentanglement by the exchange interaction. Phys. Rev. A *83*, 042331. https://doi.org/10.1103/PhysRevA.83.042331.

19. Bae, Y., Yang, K., Willke, P., Choi, T., Heinrich, A.J., and Lutz, C.P. (2018). Enhanced quantum coherence in exchange coupled spins via singlet-triplet transitions. Sci. Adv. *4*, eaau4159. https://doi.org/10.1126/sciadv.aau4159.

20. Baart, T.A., Fujita, T., Reichl, C., Wegscheider, W., and Vandersypen, L.M.K. (2017). Coherent spin-exchange via a quantum mediator. Nat. Nanotechnol. *12*, 26–30. https://doi.org/10.1038/nnano.2016.188.

21. Kandel, Y.P., Qiao, H., Fallahi, S., Gardner, G.C., Manfra, M.J., and Nichol, J.M. (2019). Coherent spin-state transfer via Heisenberg exchange. Nature *573*, 553–557. https://doi.org/10.1038/s41586-019-1566-8.

22. Ladd, T.D., Jelezko, F., Laflamme, R., Nakamura, Y., Monroe, C., and O'Brien, J.L. (2010). Quantum computers. Nature *464*, 45–53. https://doi.org/10.1038/nature08812.

23. Heinrich, A.J., Oliver, W.D., Vandersypen, L.M.K., Ardavan, A., Sessoli, R., Loss, D., Jayich, A.B., Fernandez-Rossier, J., Laucht, A., and Morello, A. (2021). Quantum-coherent nanoscience. Nat. Nanotechnol. *16*, 1318–1329. https://doi.org/10.1038/s41565-021-00994-1.

24. Khlobystov, A.N., Porfyrakis, K., Kanai, M., Britz, D.A., Ardavan, A., Shinohara, H., Dennis, T.J.S., and Briggs, G.A.D. (2004). Molecular motion of endohedral fullerenes in single-walled carbon nanotubes. Angew. Chem. Int. Ed. Engl. *43*, 1386–1389. https://doi.org/10.1002/anie.200352389.

25. Bogani, L., and Wernsdorfer, W. (2008). A perspective on combining molecular nanomagnets and carbon nanotube electronics. Inorg. Chim. Acta *361*, 3807–3819. https://doi.org/10.1016/j.ica.2008.03.074.

26. Bogani, L., Danieli, C., Biavardi, E., Bendiab, N., Barra, A.L., Dalcanale, E., Wernsdorfer, W., and Cornia, A. (2009). Single-molecule-magnet carbon-nanotube hybrids. Angew. Chem. Int. Ed. Engl. *48*, 746–750. https://doi.org/10.1002/anie.200804967.

27. Kyatskaya, S., Mascarós, J.R., Bogani, L., Hennrich, F., Kappes, M., Wernsdorfer, W., and Ruben, M. (2009). Anchoring of rare-earth-based single-molecule magnets on single-walled carbon nanotubes. J. Am. Chem. Soc. *131*, 15143–15151. https://doi.org/10.1021/ja906165e.

28. Krainov, I.V., Klier, J., Dmitriev, A.P., Klyatskaya, S., Ruben, M., Wernsdorfer, W., and Gornyi, I.V. (2017). Giant magnetoresistance in carbon nanotubes with single-molecule magnets $TbPc_2$. ACS Nano *11*, 6868–6880. https://doi.org/10.1021/acsnano.7b02014.

29. Katoh, K., Sato, J., Nakanishi, R., Ara, F., Komeda, T., Kuwahara, Y., Saito, T., Breedlove, B.K., and Yamashita, M. (2021). Terbium(III) bis-phthalocyaninato single-molecule magnet encapsulated in a single-walled carbon nanotube. J. Mater. Chem. C *9*, 10697–10704. https://doi.org/10.1039/D1TC01026C.

30. Villalva, J., Develioglu, A., Montenegro-Pohlhammer, N., Sánchez-de-Armas, R., Gamonal, A., Rial, E., García-Hernández, M., Ruiz-Gonzalez, L., Costa, J.S., Calzado, C.J., et al. (2021). Spin-state-dependent electrical conductivity in single-walled carbon nanotubes encapsulating spin-crossover molecules. Nat. Commun. *12*, 1578. https://doi.org/10.1038/s41467-021-21791-3.

31. Liu, J., and Feng, X. (2020). Synthetic tailoring of graphene nanostructures with zigzag-edged topologies: progress and perspectives. Angew. Chem. Int. Ed. Engl. *59*, 23386–23401. https://doi.org/10.1002/anie.202008838.

32. Zeng, W., and Wu, J. (2021). Open-shell graphene fragments. Chem *7*, 358–386. https://doi.org/10.1016/j.chempr.2020.10.009.

33. Cervetti, C., Rettori, A., Pini, M.G., Cornia, A., Repollés, A., Luis, F., Dressel, M., Rauschenbach, S., Kern, K., Burghard, M., and Bogani, L. (2016). The classical and quantum dynamics of molecular spins on graphene. Nat. Mater. *15*, 164–168. https://doi.org/10.1038/nmat4490.

34. Slota, M., Keerthi, A., Myers, W.K., Tretyakov, E., Baumgarten, M., Ardavan, A., Sadeghi, H., Lambert, C.J., Narita, A., Müllen, K., and Bogani, L. (2018). Magnetic edge states and coherent manipulation of graphene

nanoribbons. Nature *557*, 691–695. https://doi.org/10.1038/s41586-018-0154-7.

35. Meunier, V., Souza Filho, A.G., Barros, E.B., and Dresselhaus, M.S. (2016). Physical properties of low-dimensional sp^2-based carbon nanostructures. Rev. Mod. Phys. *88*, 025005. https://doi.org/10.1103/RevModPhys.88.025005.

36. Crossley, M.J., and Burn, P.L. (1991). An approach to porphyrin-based molecular wires: synthesis of a bis(porphyrin)tetraone and its conversion to a linearly conjugated tetrakisporphyrin system. J. Chem. Soc. Chem. Commun. 1569–1571. https://doi.org/10.1039/C39910001569.

37. Anderson, H.L. (1994). Conjugated porphyrin ladders. Inorg. Chem. *33*, 972–981. https://doi.org/10.1021/ic00083a022.

38. Lin, V.S.-Y., DiMagno, S.G., and Therien, M.J. (1994). Highly conjugated, acetylenyl bridged porphyrins: new models for light-harvesting antenna systems. Science *264*, 1105–1111. https://doi.org/10.1126/science.8178169.

39. Taylor, P.N., Huuskonen, J., Aplin, R.T., Anderson, H.L., Huuskonen, J., Rumbles, G., and Williams, E. (1998). Conjugated porphyrin oligomers from monomer to hexamer. Chem. Commun. 909–910. https://doi.org/10.1039/A801031E.

40. Tsuda, A., and Osuka, A. (2001). Fully conjugated porphyrin tapes with electronic absorption bands that reach into infrared. Science *293*, 79–82. https://doi.org/10.1126/science.1059552.

41. Tsuda, A., Furuta, H., and Osuka, A. (2001). Syntheses, structural characterizations, and optical and electrochemical properties of directly fused diporphyrins. J. Am. Chem. Soc. *123*, 10304–10321. https://doi.org/10.1021/ja0110933.

42. Leary, E., Limburg, B., Alanazy, A., Sangtarash, S., Grace, I., Swada, K., Esdaile, L.J., Noori, M., González, M.T., Rubio-Bollinger, G., et al. (2018). Bias-driven conductance increase with length in porphyrin tapes. J. Am. Chem. Soc. *140*, 12877–12883. https://doi.org/10.1021/jacs.8b06338.

43. Sedghi, G., Esdaile, L.J., Anderson, H.L., Martin, S., Bethell, D., Higgins, S.J., and Nichols, R.J. (2012). Comparison of the conductance of three types of porphyrin-based molecular wires: β,meso,β-fused tapes, meso-butadiyne-linked and twisted meso-meso linked oligomers. Adv. Mater. *24*, 653–657. https://doi.org/10.1002/adma.201103109.

44. Li, Z., Park, T.H., Rawson, J., Therien, M.J., and Borguet, E. (2012). Quasi-Ohmic single molecule charge transport through highly conjugated meso-to-meso ethyne-bridged porphyrin wires. Nano Lett. *12*, 2722–2727. https://doi.org/10.1021/nl2043216.

45. Ikeue, T., Furukawa, K., Hata, H., Aratani, N., Shinokubo, H., Kato, T., and Osuka, A. (2005). The importance of a β−β bond for long-range antiferromagnetic coupling in directly linked copper(II) and silver(II) diporphyrins. Angew. Chem. Int. Ed. Engl. *44*, 6899–6901. https://doi.org/10.1002/anie.200501943.

46. Wili, N., Richert, S., Limburg, B., Clarke, S.J., Anderson, H.L., Timmel, C.R., and Jeschke, G. (2019). ELDOR-detected NMR beyond hyperfine couplings: a case study with Cu(II)-porphyrin dimers. Phys. Chem. Chem. Phys. *21*, 11676–11688. https://doi.org/10.1039/C9CP01760G.

47. Wang, R., Brugh, A.M., Rawson, J., Therien, M.J., and Forbes, M.D.E. (2017). Alkyne-bridged multi[copper(II) porphyrin structures: nuances of orbital symmetry in long-range, through-bond mediated, isotropic spin exchange interactions. J. Am. Chem. Soc. *139*, 9759–9762. https://doi.org/10.1021/jacs.7b03252.

48. Le Roy, J.J., Cremers, J., Thomlinson, I.A., Slota, M., Myers, W.K., Horton, P.H., Coles, S.J., Anderson, H.L., and Bogani, L. (2018). Tailored homo- and hetero- lanthanide porphyrin dimers: a synthetic strategy for integrating multiple spintronic functionalities into a single molecule. Chem. Sci. *9*, 8474–8481. https://doi.org/10.1039/C8SC03762K.

49. Van Raden, J.M., Alexandropoulos, D.I., Slota, M., Sopp, S., Matsuno, T., Thompson, A.L., Isobe, H., Anderson, H.L., and Bogani, L. (2022). Singly and triply linked magnetic porphyrin lanthanide arrays. J. Am. Chem. Soc. *144*, 8693–8706. https://doi.org/10.1021/jacs.2c02084.

50. Pozo, I., Lombardi, F., Alexandropoulos, D.I., Kong, F., Deng, J.-R., Horton, P.N., Coles, S.J., Myers, W.K., Bogani, L., and Anderson, H.L. (2022). Conjugated porphyrin tapes as quantum mediators for vanadyl qubits. Preprint at ChemRxiv. https://doi.org/10.26434/chemrxiv-2022-1v5b4.

51. Ranieri, D., Santanni, F., Privitera, A., Albino, A., Salvadori, E., Chiesa, M., Totti, F., Sorace, L., and Sessoli, R. (2022). An exchange coupled meso-meso linked vanadyl porphyrin dimer for quantum information processing. Chem. Sci. *14*, 61–69. https://doi.org/10.1039/D2SC04969D.

52. Buchler, J.W., Eikelmann, G., Puppe, L., Rohbock, K., Schneehage, H.H., and Weck, D. (1971). Metallkomplexe mit Tetrapyrrol-Liganden, III. Darstellung von Metallkomplexen des Octaäthylporphins aus Metall-acetylacetonaten. Justus Liebigs Ann. Chem. *745*, 135–151. https://doi.org/10.1002/jlac.19717450117.

53. Bonnett, R., Brewer, P., Noro, K., and Noro, T. (1978). Chemistry of vanadyl porphyrins. Tetrahedron *34*, 379–385. https://doi.org/10.1016/S0040-4020(01)93596-3.

54. Bencosme, S., Labady, M., and Romero, C. (1986). Synthesis of vanadylporphyrins revisited. Inorg. Chim. Acta *123*, 15–17. https://doi.org/10.1016/S0020-1693(00)81309-2.

55. Ryan, A., Gehrold, A., Perusitti, R., Pintea, M., Fazekas, M., Locos, O.B., Blaikie, F., and Senge, M.O. (2011). Porphyrin dimers and arrays. Eur. J. Org. Chem. *2011*, 5817–5844. https://doi.org/10.1002/ejoc.201100642.

56. The plane of the porphyrin is defined as the mean plane of the 24-atom porphyrin core. In cases with disorder, sites of highest occupancy are used when analyzing crystal structures.

57. Molinaro, F.S., and Ibers, J.A. (1976). Crystal and molecular structure of 2,3,7,8,12,13,17,18-octaethylporphinatooxovanadium(IV). Inorg. Chem. *15*, 2278–2283. https://doi.org/10.1021/ic50163a057.

58. Drew, M.G.B., Mitchell, P.C.H., and Scott, C.E. (1984). Crystal and molecular structure of three oxovanadium(IV) porphyrins: oxovanadium tetraphenylporphyrin(I), oxovanadium(IV) etioporphyrin(II) and the 1:2 adduct of (II) with 1,4-dihydroxybenzene(III). Hydrogen bonding involving the VO group. Relevance to catalytic demetallisation. Inorg. Chim. Acta *82*, 63–68. https://doi.org/10.1016/S0020-1693(00)82539-6.

59. Smith, M.J., Blake, I.M., Clegg, W., and Anderson, H.L. (2018). Push-pull quinoidal porphyrins. Org. Biomol. Chem. *16*, 3648–3654. https://doi.org/10.1039/C8OB00491A.

60. Duncan, T.V., Frail, P.R., Miloradovic, I.R., and Therien, M.J. (2010). Excitation of highly conjugated (porphinato)palladium(II) and (porphinato)platinum(II) oligomers produces long-lived, triplet states at unit quantum yield that absorb strongly over broad spectral domains of the NIR. J. Phys. Chem. B *114*, 14696–14702. https://doi.org/10.1021/jp102901u.

61. Peeks, M.D., Neuhaus, P., and Anderson, H.L. (2016). Experimental and computational evaluation of the barrier to torsional rotation in a butadiyne-linked porphyrin dimer. Phys. Chem. Chem. Phys. *18*, 5264–5274. https://doi.org/10.1039/C5CP06167A.

62. Hutin, M., Sprafke, J.K., Odell, B., Anderson, H.L., and Claridge, T.D.W. (2013). A discrete three-layer stack aggregate of a linear porphyrin tetramer: solution-phase structure elucidation by NMR and X-ray scattering. J. Am. Chem. Soc. *135*, 12798–12807. https://doi.org/10.1021/ja406015r.

63. Mannikko, D., and Stoll, S. (2019). Vanadyl porphyrin speciation based on submegahertz ligand proton hyperfine couplings. Energy Fuels *33*, 4237–4243. https://doi.org/10.1021/acs.energyfuels.9b00867.

64. Roessler, M.M., and Salvadori, E. (2018). Principles and applications of EPR spectroscopy in the chemical sciences. Chem. Soc. Rev. *47*, 2534–2553. https://doi.org/10.1039/C6CS00565A.

65. Munzarová, M.L., Kubácek, P., and Kaupp, M. (2000). Mechanisms of EPR hyperfine coupling in transition metal complexes. J. Am. Chem. Soc. *122*, 11900–11913. https://doi.org/10.1021/ja002062v.

66. Reitz, D.C., and Weissman, S.I. (1960). Spin exchange in biradicals. J. Chem. Phys. *33*, 700–704. https://doi.org/10.1063/1.1731241.

67. Atzori, M., Chiesa, A., Morra, E., Chiesa, M., Sorace, L., Carretta, S., and Sessoli, R. (2018). A two-Qubit molecular architecture for electron-mediated nuclear quantum simulation. Chem. Sci. *9*, 6183–6192. https://doi.org/10.1039/C8SC01695J.

68. Borilovic, I., Alonso, P.J., Roubeau, O., and Aromí, G. (2020). A bis-vanadyl coordination complex as a 2-Qubit quantum gate. Chem.

Commun. (Camb) *56*, 3139–3142. https://doi.org/10.1039/C9CC09817H.

69. Thanabal, V., and Krishnan, V. (1982). Cation-induced crown porphyrin dimers of oxovanadium(IV). Inorg. Chem. *21*, 3606–3613. https://doi.org/10.1021/ic00140a006.

70. Branca, M., Micera, G., Sanna, D., Dessì, A., and Kozłowski, H. (1990). Stabilization of the open-chain structure of D-galacturonic acid in a dimeric complex with oxovanadium(IV). J. Chem. Soc. Dalton Trans. 1997–1999. https://doi.org/10.1039/DT9900001997.

71. Zoroddu, M.A., and Masia, A. (1997). A novel dimeric oxovanadium (IV) species identified in Saccharomyces cerevisiae cells. Biochim. Biophys. Acta *1358*, 249–254. https://doi.org/10.1016/S0167-4889(97)00074-8.

72. The dipolar coupling (*D*) was calculated according to the formula: $D = -3\mu_0 \cdot (g_e \cdot \beta_e)^2 / (8 \cdot \pi \cdot h \cdot r^3)$ where $\mu_0 = 4\pi \times 10^{-7}$ (H/m), $g_e = 2.0023$, $\beta_e = 9.27 \times 10^{-24}$ (J/T), *h* is the Planck constant, and *r* is the distance between metal centers, 8.466 and 8.402 Å from the X-ray crystallography.

73. $X_M T = [Ng^2\beta^2/(3k)]S(S+1)$, where $X_M T$ is the molar magnetic susceptibility at 300 K, *N* is the number of spins, *g* is the Landé Factor, β is the Bohr magneton, and *k* is the Boltzmann constant, and $M(N\mu B) = g \cdot S$, where *g* is the Landé factor, and *S* the spin number. See Khan, O. (1993). Molecular Magnetism. (Wiley-VCH). ISBN 3-527-89566-3.

74. Kuzhelev, A.A., Krumkacheva, O.A., Ivanov, M.Y., Prikhod'ko, S.A., Adonin, N.Y., Tormyshev, V.M., Bowman, M.K., Fedin, M.V., and Bagryanskaya, E.G. (2018). Pulse EPR of triarylmethyl probes: a new approach for the investigation of molecular motions in soft matter. J. Phys. Chem. B *122*, 8624–8630. https://doi.org/10.1021/acs.jpcb.8b07714.

75. Atzori, M., Tesi, L., Benci, S., Lunghi, A., Righini, R., Taschin, A., Torre, R., Sorace, L., and Sessoli, R. (2017). Spin dynamics and low energy vibrations: insights from vanadyl-based potential molecular qubits. J. Am. Chem. Soc. *139*, 4338–4341. https://doi.org/10.1021/jacs.7b01266.

76. Wedge, C.J., Timco, G.A., Spielberg, E.T., George, R.E., Tuna, F., Rigby, S., McInnes, E.J.L., Winpenny, R.E.P., Blundell, S.J., and Ardavan, A. (2012). Chemical engineering of molecular qubits. Phys. Rev. Lett. *108*, 107204. https://doi.org/10.1103/PhysRevLett.108.107204.

77. Ferrando-Soria, J., Magee, S.A., Chiesa, A., Carretta, S., Santini, P., Vitorica-Yrezabal, I.J., Tuna, F., Whitehead, G.S., Sproules, S., Lancaster, K.M., et al. (2016). Switchable interaction in molecular double qubits. Chem *1*, 727–752. https://doi.org/10.1016/j.chempr.2016.10.001.

78. Cervetti, C., Heintze, E., and Bogani, L. (2014). Interweaving spins with their environment: novel inorganic nanohybrids with controllable magnetic properties. Dalton Trans. *43*, 4220–4232. https://doi.org/10.1039/C3DT52650J.

79. Mergenthaler, M., Liu, J., Le Roy, J.J., Ares, N., Thompson, A.L., Bogani, L., Luis, F., Blundell, S.J., Lancaster, T., Ardavan, A., and Briggs, G.D. (2017). Strong coupling of microwave photons to antiferromagnetic fluctuations in an organic magnet. Phys. Rev. Lett. *119*, 147701. https://doi.org/10.1103/PhysRevLett.119.147701.

80. Urtizberea, A., Natividad, E., Alonso, P.J., Pérez-Martínez, L., Andrés, M.A., Gascón, I., Gimeno, I., Luis, F., and Roubeau, O. (2020). Vanadyl spin Qubit 2D arrays and their integration on superconducting resonators. Mater. Horiz. *7*, 885–897. https://doi.org/10.1039/C9MH01594A.

81. Carretta, S., Zueco, D., Chiesa, A., Gómez-León, Á., and Luis, F. (2021). A perspective on scaling up quantum computation with molecular spins. Appl. Phys. Lett. *118*, 240501. https://doi.org/10.1063/5.0053378.

82. Ouyang, M., and Awschalom, D.D. (2003). Coherent spin transfer between molecularly bridged quantum dots. Science *301*, 1074–1078. https://doi.org/10.1126/science.1086963.

83. Yoshizawa, K. (2012). An orbital rule for electron transport in molecules. Acc. Chem. Res. *45*, 1612–1621. https://doi.org/10.1021/ar300075f.

84. Thiele, S., Balestro, F., Ballou, R., Klyatskaya, S., Ruben, M., and Wernsdorfer, W. (2014). Electrically driven nuclear spin resonance in single-molecule magnets. Science *344*, 1135–1138. https://doi.org/10.1126/science.1249802.

85. Frisenda, R., Stefani, D., and van der Zant, H.S.J. (2018). Quantum transport through a single conjugated rigid molecule, a mechanical break junction study. Acc. Chem. Res. *51*, 1359–1367. https://doi.org/10.1021/acs.accounts.7b00493.

86. Gehring, P., Thijssen, J.M., and van der Zant, H.S.J. (2019). Single-molecule quantum-transport phenomena in break junctions. Nat. Rev. Phys. *1*, 381–396. https://doi.org/10.1038/s42254-019-0055-1.

87. Schosser, W.M., Hsu, C., Zwick, P., Beltako, K., Dulić, D., Mayor, M., van der Zant, H.S.J., and Pauly, F. (2022). Mechanical conductance tunability of a porphyrin–cyclophane single-molecule junction. Nanoscale *14*, 984–992. https://doi.org/10.1039/D1NR06484C.

88. Sun, Q., Mateo, L.M., Robles, R., Lorente, N., Ruffieux, P., Bottari, G., Torres, T., and Fasel, R. (2021). Bottom-up fabrication and atomic-scale characterization of triply linked, laterally π-extended porphyrin nanotapes*. Angew. Chem. Int. Ed. Engl. *60*, 16208–16214. https://doi.org/10.1002/anie.202105350.

89. Wende, H., Bernien, M., Luo, J., Sorg, C., Ponpandian, N., Kurde, J., Miguel, J., Piantek, M., Xu, X., Eckhold, P., et al. (2007). Substrate-induced magnetic ordering and switching of iron porphyrin molecules. Nat. Mater. *6*, 516–520. https://doi.org/10.1038/nmat1932.

90. Zoppellaro, G., Bakandritsos, A., Tuček, J., Błoński, P., Susi, T., Lazar, P., Bad'ura, Z., Steklý, T., Opletalová, A., Otyepka, M., and Zbořil, R. (2019). Microwave energy drives "on-off-on" spin-switch behavior in nitrogen-doped graphene. Adv. Mater. *31*, e1902587. https://doi.org/10.1002/adma.2019s41467-022-3190987.

91. Pei, T., Thomas, J.O., Sopp, S., Tsang, M.Y., Dotti, N., Baugh, J., Chilton, N.F., Cardona-Serra, S., Gaita-Ariño, A., Anderson, H.L., and Bogani, L. (2022). Exchange-induced spin polarization in a single magnetic molecule junction. Nat. Commun. *13*, 4506. https://doi.org/10.1038/s41467-022-31909-w.

92. Tsukagoshi, K., Alphenaar, B.W., and Ago, H. (1999). Coherent transport of electron spin in a ferromagnetically contacted carbon nanotube. Nature *401*, 572–574. https://doi.org/10.1038/44108.

93. Petta, J.R., Slater, S.K., and Ralph, D.C. (2004). Spin-dependent transport in molecular tunnel junctions. Phys. Rev. Lett. *93*, 136601. https://doi.org/10.1103/PhysRevLett.93.136601.

94. Flentje, H., Mortemousque, P.A., Thalineau, R., Ludwig, A., Wieck, A.D., Bäuerle, C., and Meunier, T. (2017). Coherent long-distance displacement of individual electron spins. Nat. Commun. *8*, 501. https://doi.org/10.1038/s41467-017-00534-3.

95. Qiao, H., Kandel, Y.P., Deng, K., Fallahi, S., Gardner, G.C., Manfra, M.J., Barnes, E., and Nichol, J.M. (2020). Coherent multispin exchange coupling in a quantum-dot spin chain. Phys. Rev. X *10*, 031006. https://doi.org/10.1103/PhysRevX.10.031006.

96. Mortemousque, P.A., Chanrion, E., Jadot, B., Flentje, H., Ludwig, A., Wieck, A.D., Urdampilleta, M., Bäuerle, C., and Meunier, T. (2021). Coherent control of individual electron spins in a two-dimensional quantum dot array. Nat. Nanotechnol. *16*, 296–301. https://doi.org/10.1038/s41565-020-00816-w.

97. Li, J.R., Matsuda, K., Miller, C., Carroll, A.N., Tobias, W.G., Higgins, J.S., and Ye, J. (2023). Tunable itinerant spin dynamics with polar molecules. Nature *614*, 70–74. https://doi.org/10.1038/s41586-022-05479-2.

98. Dikarov, E., Zgadzai, O., Artzi, Y., and Blank, A. (2016). Direct measurement of the flip-flop rate of electron spins in the solid state. Phys. Rev. Appl. *6*, 044001. https://doi.org/10.1103/PhysRevApplied.6.044001.

99. Tyryshkin, A.M., Tojo, S., Morton, J.J.L., Riemann, H., Abrosimov, N.V., Becker, P., Pohl, H.J., Schenkel, T., Thewalt, M.L.W., Itoh, K.M., and Lyon, S.A. (2011). Electron spin coherence exceeding seconds in high-purity silicon. Nat. Mater. *11*, 143–147. https://doi.org/10.1038/nmat3182.

100. Bian, X., Chen, Z., Sowa, J.K., Evangeli, C., Limburg, B., Swett, J.L., Baugh, J., Briggs, G.A.D., Anderson, H.L., Mol, J.A., and Thomas, J.O. (2022). Charge-state dependent vibrational relaxation in a single-molecule junction. Phys. Rev. Lett. *129*, 207702. https://doi.org/10.1103/PhysRevLett.129.207702.

101. Chen, Z., Deng, J.R., Hou, S., Bian, X., Swett, J.L., Wu, Q., Baugh, J., Bogani, L., Briggs, G.A.D., Mol, J.A., et al. (2023). Phase-coherent charge transport through a porphyrin nanoribbon. J. Am. Chem. Soc. *145*, 15265–15274. https://doi.org/10.1021/jacs.3c02451.